Bone 120 (2019) 75–84

Contents lists available at ScienceDirect

Bone

journal homepage: www.elsevier.com/locate/bone

Full Length Article

Findings as a starting point to unravel the underlying mechanisms of in vivo interactions involving Wnt10a in bone, fat and muscle

Manabu Tsukamoto[a], Ke-Yong Wang[b,*], Takashi Tasaki[c], Yoichi Murata[a], Yasuaki Okada[a], Yoshiaki Yamanaka[a], Eiichiro Nakamura[a], Sohsuke Yamada[d], Hiroto Izumi[e], Qian Zhou[f], Kagaku Azuma[f], Yasuyuki Sasaguri[c,g], Kimitoshi Kohno[h], Akinori Sakai[a]

[a] Department of Orthopaedic Surgery, School of Medicine, University of Occupational and Environmental Health University, 1-1 Iseigaoka, Yahatanishi-ku, Kitakyushu 807-8555, Japan
[b] Shared-Use Research Center, School of Medicine, University of Occupational and Environmental Health, 1-1 Iseigaoka, Yahatanishi-ku, Kitakyushu 807-8555, Japan
[c] Department of Pathology and Cell Biology, School of Medicine, University of Occupational and Environmental Health, 1-1 Iseigaoka, Yahatanishi-ku, Kitakyushu 807-8555, Japan
[d] Department of Pathology and Laboratory Medicine, Kanazawa Medical University, 1-1 Uchinada, Ishikawa 920-0293, Japan
[e] Department of Occupational Pneumology, School of Medicine, University of Occupational and Environmental Health, 1-1 Iseigaoka, Yahatanishi-ku, Kitakyushu 807-8555, Japan
[f] Department of Anatomy, School of Medicine, University of Occupational and Environmental Health, 1-1 Iseigaoka, Yahatanishi-ku, Kitakyushu 807-8555, Japan
[g] Laboratory of Pathology, Fukuoka Tokushukai Hospital, Fukuoka 816-0864, Japan
[h] Asahi-Matsumoto Hospital, Kitakyushu 800-0242, Japan

ARTICLE INFO

Keywords:
Gdf8
Myostatin
Osteogenesis
Beige adipogenesis
Muscle fiber

ABSTRACT

Wnt10a is a member of the WNT family. Although deficiency of this gene causes symptoms related to teeth, hair, nails, and skin, we recently demonstrated a new phenotype of Wnt10a knockout (KO) mice involving bone and fat. The in vivo effect of the Wnt10a gene on bone and fat is unclear, and the relationship between bone/fat and muscle in Wnt10a signaling is also interesting. We aimed to evaluate the tissue changes in Wnt10a KO mice compared to wild-type mice and show the findings as a starting point to unravel the underlying mechanisms of in vivo interactions involving Wnt10a in bone, fat and muscle. Trabecular bone loss in the lower limbs of Wnt10a mice and decreased bone mineralization were observed. The adipose tissue in bone marrow was also decreased, and adipocyte differentiation was reduced. The body fat mass in Wnt10a KO mice was decreased, and white adipocytes in subcutaneous fat were converted to beige adipocytes. The muscle weight of the lower limbs was not decreased despite trabecular bone loss, but Gdf8/myostatin expression was reduced in the subcutaneous fat and gastrocnemius muscles of Wnt10a KO mice. Thus, in vivo deletion of Wnt10a inhibited osteogenic activity, promoted beige adipogenesis of white adipocytes and maintained muscle mass. These results suggest that regulation of Gdf8 by Wnt10a may help maintain the muscle mass of Wnt10a KO mice. This study was the first to histologically evaluate the bone, fat and muscle phenotypes of Wnt10a KO mice. The results of this study, which were obtained by investigating the three tissues together, could influence the understanding of in vivo interactions involving the Wnt10a gene.

1. Introduction

Wnt10a is a member of the WNT family. A typical disease caused by deficiency of this gene is odonto-onycho-dermal dysplasia, which has symptoms related to teeth, hair, nails, and skin [1]. Recent studies have reported phenotypes related to teeth and skin in Wnt10a knockout (KO) mice [2,3], and our group has also examined wound healing in the skin [4,5]. In this study, the Wnt10a KO mouse demonstrated a new

Abbreviations: Wnt10a, wingless related MMTV integration site 10a; RUNX2, runt-related transcription factor 2; Col1a1, collagen type 1 alpha 1; CEBPα, CCAAT/enhancer-binding protein alpha; CEBPβ, CCAAT/enhancer-binding protein beta; PPARγ, peroxisome proliferator-activated receptor γ; FABP4, fatty acid-binding protein 4; Cidea, cell death activator; Cox5b, cytochrome *c* oxidase subunit 5b; Dio2, type II iodothyronine deiodinase; Elovl3, elongation of very long chain fatty acid 3; UCP1, uncoupling protein 1; PRDM16, PR domain containing 16; MuRF1, muscle RING-finger protein-1; Myf5, myogenic factor 5; MyoD, myogenic differentiation; MyHC, myosin heavy chain; Gdf8, growth differentiation factor 8

* Corresponding author.
E-mail address: kywang@med.uoeh-u.ac.jp (K.-Y. Wang).

https://doi.org/10.1016/j.bone.2018.10.009
Received 13 July 2018; Received in revised form 8 October 2018; Accepted 8 October 2018
Available online 11 October 2018

phenotype in bone and fat: a decrease in femur bone mineral density and body fat mass [4].

No reports have investigated the influence of Wnt10a on bone and fat in vivo, although there have been several in vitro studies. Cawthorn et al. [6] reported that Wnt6, Wnt10a and Wnt10b inhibit adipogenesis and stimulate osteoblastogenesis through a β-catenin-dependent mechanism. In addition, Chen et al. [7] reported that inhibiting DNA methylation switches adipogenesis to osteoblastogenesis by activating Wnt10a. Given these findings, we hypothesized that osteoblastogenesis is inhibited and adipogenesis is promoted in Wnt10a KO mice, but the mice in our study unexpectedly showed decreased body fat mass.

However, a previous study supported our results. In osteocyte-specific Gsα KO mice with high expression of sclerostin, a WNT signal inhibitor secreted from osteocytes, the body fat mass was decreased, and beige adipogenesis of white adipocytes was observed [8]. Surprisingly, the muscle mass measured by dual-energy X-ray absorption (DXA) was significantly higher in the KO mice than in the wild-type (WT) mice. WNT signals are involved in the development of muscle during the growth phase and in the regulation of slow- versus fast-twitch myofiber formation in adults [9]. It is unlikely that muscle mass will increase by suppressing WNT signaling, since WNT signaling activation is expected to have a positive effect on muscle fibers based on previous studies.

It is important to investigate the in vivo changes in tissues altogether because there is an interaction among bone, fat and muscle. Since the influence of Wnt10a on bone, fat and muscle in vivo is unclear, we hypothesized that the results obtained by investigating the three tissues together will help to elucidate the in vivo influence of the Wnt10a gene. The purpose of this study was to evaluate the changes in each tissue in Wnt10a KO mice compared to WT mice, and the findings were considered a starting point to unravel the underlying mechanisms of in vivo interactions involving Wnt10a in bone, fat and muscle.

2. Materials and methods

2.1. Wnt10a knockout mice

Wnt10a knockout mice were generated as previously described [4]. Experiments were performed on 16-week-old male Wnt10a KO mice (KO group) and WT littermates (WT group), which were used as a control group (n = 5 to 7 mice per experiment). Animals were provided diet and water ad libitum and maintained on a 12-h light/dark cycle. All animal experiments were conducted according to the guidelines of the Laboratory Animal Research Center at the University of Occupational and Environmental Health School of Medicine. The Ethics Committee of Animal Care and Experimentation at the University of Occupational and Environmental Health (Japan) approved the protocols. All experiments were performed according to the Institutional Guidelines for Animal Experiments and the Law (no. 105) and Notification (no. 6) of the Japanese Government. The investigation conformed to the Guide for the Care and Use of Laboratory Animals published by the US National Institutes of Health (NIH Publication No. 85-23, revised 1996).

2.2. Micro-CT

2.2.1. Bone microstructure

The trabecular bones of the right distal femoral metaphysis were analyzed by a microcomputed tomography (micro-CT) system (CosmoScan GX; Rigaku, Tokyo, Japan) with a resolution of $10 \times 10 \times 10\ \mu m^3$ (90 kVp, 88 μA, 533.33 ms integration time) and a metaphyseal volume of interest height of 1.0 mm, commencing 0.5 mm proximal to the growth plate. Cortical bone was assessed in 50 slices of the femur midshaft. A median-type filter was utilized (Kernel size; $5 \times 5 \times 5$). The minimum threshold for bone was 334 mg/cm^3, which was determined through correlations with phantoms of known density. The bone microstructure parameters in the trabecular bones of distal femoral metaphysis were evaluated using Analyze 12.0 software (AnalyzeDirect, Inc., KS, USA) and presented as follows: trabecular bone volume (BV/TV: %), trabecular thickness (Tb.Th: mm), trabecular separation (Tb.Sp: mm), trabecular number (Tb.N: 1/mm), structure model index (SMI), connectivity density (Conn.D: 1/mm^3), total cross-sectional area inside the periosteal envelope (Tt.Ar: mm^2), cortical bone area (Ct.Ar: mm^2), cortical area fraction (Ct.Ar/Tt.Ar: %), and average cortical thickness (Ct.Th: mm). Parameters are reported according to published guidelines [10].

2.2.2. Fat volume

Mice were anesthetized by intraperitoneal injection of 0.3 mg/kg medetomidine (Kyoritsu Seiyaku Corporation, Tokyo, Japan), 1.0 mg/kg midazolam (Astellas Pharma Inc., Tokyo, Japan), and 5.0 mg/kg butorphanol (Meiji Seika Pharma Co., Ltd., Tokyo, Japan) before undergoing micro-CT scanning. CT images of visceral and subcutaneous fat were acquired by micro-CT with a resolution of $120 \times 120 \times 120\ \mu m^3$. The CT images of body fat were also visualized using Analyze 12.0 software. The total and fat volume in the body was measured from the base of the ensiform cartilage to the pelvic floor, and the fat volume was further distinguished into visceral and subcutaneous fat [4,11].

2.3. Bone histomorphometry

Bone histomorphometric analysis of nondecalcified specimens from the right proximal tibia was performed as described previously [12]. Regarding the parameters, the BV/TV (%), osteoid surface (OS/BS: %), osteoblast surface (Ob.S/BS: %) and adipose tissue volume per total marrow volume (AV/MV: %) were determined, and the mineralizing surface (MS/BS: %), mineral apposition rate (MAR: μm/day) and surface referent bone formation rate (BFR/BS: mm^3/mm^2/year) were obtained using luminescence microscopy. Regarding the bone resorption parameters, the osteoclast surface (Oc.S/BS: %) and osteoclast number (Oc.N/BS: #/mm) were measured in the right proximal tibia. The cells that formed resorption lacunae on the surface of the trabeculae and contained two or more nuclei were identified as osteoclasts [12]. The abbreviations for the histomorphometric parameters were derived from the recommendations of the Histomorphometry Nomenclature Committee of the American Society for Bone and Mineral Research [13,14].

2.4. Cell cultures

2.4.1. ALP-positive CFU-f

Bone marrow from the bilateral femurs and tibias was flushed from the proximal end of the metaphysis with 5 ml of α-MEM. For determination of the alkaline phosphatase (ALP)-positive colony forming unit-fibroblastic (CFU-f) colony formation, marrow cells were plated at 1×10^5 cells/well in 6-well plates (Iwaki, Tokyo, Japan) and α-MEM containing 10% fetal bovine serum (FBS), 2.0 g/l $NaHCO_3$, 100 μg/ml streptomycin, 100 U/ml penicillin, 0.25 μg/ml amphotericin B and 50 μg/ml ascorbic acid (Wako Pure Chemicals, Osaka, Japan). On day 10, the CFU-f colonies were fixed with fixation solution and treated with a tablet of substrate for ALP (TRACP & ALP Double-stain Kit; TaKaRa, Shiga, Japan) dissolved in 10 ml of ddw for 30 min at 37 °C. Colonies containing 50 cells were defined as CFU-f. We counted the total and ALP-positive CFU-f colonies with the culture dishes backlit at 5-fold magnification [15–18].

2.4.2. Mineralized nodule formation

Bone marrow cells were seeded onto 24-well plates (Iwaki) at a concentration of 1×10^5 cells in 0.5 ml of α-MEM containing 10% FBS, 2.0 g/l $NaHCO_3$, 100 μg/ml streptomycin, 100 U/ml penicillin, 0.25 μg/ml amphotericin B, 50 μg/ml ascorbic acid and 10 mM sodium β-glycerophosphate (Sigma). On day 21 of culture, cells were fixed for 24 h

in 10% formalin and stained for 15 min with a saturated solution of Alizarin Red (Sigma). The mineralization area (mm^2) was measured using ImageJ software (NIH) on a Macintosh computer [19,20].

2.4.3. Oil Red O-positive CFU-f

The flushed bone marrow cells were seeded onto 6-well plates (Iwaki) at a concentration of 1×10^5 cells/ml in 2 ml of α-MEM supplemented with 10% FBS, 10^{-7} M dexamethasone (Sigma-Aldrich), 0.5 mM isobutyl-1-methylxanthine (Sigma-Aldrich), and 50 μM indomethacin (WAKO, Tokyo, Japan). On day 21, these cultured cells were fixed in 4% PFA and stained with Oil Red O (Sigma-Aldrich) solution. The number of Oil Red O-positive colonies was then counted with the culture dishes backlit at 5-fold magnification [21,22].

2.5. RT-PCR

2.5.1. A isolation and first-strand cDNA synthesis

RNA isolation was performed as previously described [12,23]. First-strand cDNA was reverse transcribed from total RNA (1 μg) using Moloney murine leukemia reverse transcriptase (SuperScript II; Life Technologies, Rockville, MD) and oligo(dT) 12–18 primers (Life Technologies).

2.5.2. Quantitative real-time PCR

Quantitative real-time PCR analysis was performed using an iCycler apparatus (Bio-Rad Laboratories, Hercules, CA, USA) with iCycler Optical System Software version 3.1 (Bio-Rad). The quantitative PCR reactions for Wnt10a, β-catenin, RUNX2, osterix, Col1a1, osteocalcin, CEBPα, CEBPβ, PPARγ, FABP4, Cidea, Cox5b, Dio2, Elovl3, UCP1, PRDM16, atrogin-1, MuRF1, Myf5, MyoD, myogenin, MyHC, Gdf8 and β-actin were performed in 10 μl containing 5 ng of cDNA, 0.5 pM primers, and 5 μl of iQ SYBR Green Supermix (Bio-Rad). The primers used in this study were designed using Primer3 software and synthesized at Sigma-Aldrich Japan K.K. Genosys Division (Hokkaido, Japan). β-actin served as an internal control. The amplification conditions were an initial 3 min at 95 °C and 40–50 cycles of denaturation at 95 °C for 30 s, annealing at 65 °C for 30 s, and extension at 72 °C for 30 s. The mRNA expression levels were normalized with β-actin mRNA expression levels and expressed as relative values (fold change) to the expression levels in WT mice.

2.6. Weight of adipose and muscular tissues

From 1 to 12 months of age, KO mice displayed significantly lower body weights, as reflected by essential growth retardation, than WT mice [4]. Absolute measurements were normalized to total body weights to account for decreased body weights in the KO mice. Absolute weights of individual organs (inguinal and gonadal white adipose tissue and brown adipose tissue at the scapular region, pancreas, quadriceps, gastrocnemius, plantaris, and soleus muscle) were measured during necropsy and normalized to total body weights.

2.7. Immunohistochemical staining of adipose tissue

White adipose tissues from euthanized mice were fixed in 4% PFA. Tissues were embedded in paraffin and then sectioned at 4-μm thickness. For immunohistochemistry, paraffin-embedded tissue sections were deparaffinized in xylene and ethanol. Antigen retrieval was performed by using 0.01% proteinase (SIGMA, Tokyo, Japan) or by heat-mediated antigen retrieval in pH 6 citrate buffer. Endogenous peroxidase activity was quenched using H_2O_2, and sections were further treated with Protein Block Serum-Free (Dako, Tokyo, Japan). Each section was incubated overnight at 4 °C with rabbit polyclonal anti-Wnt10a antibody (dilution 1:5000), rabbit polyclonal anti-β-catenin antibody (dilution 1:500, AC 121 °C; Abcam, Tokyo, Japan) or rabbit polyclonal antibody against UCP1 (dilution 1:200, Abcam, Tokyo, Japan). After the primary antibody was washed off, tissues were incubated with biotin-conjugated anti-rabbit or anti-goat secondary antibody (Histofine Simple Stein mouse MAX-PO, Nichirei, Tokyo, Japan) for 30 min. The peroxidase signal was then developed using DAB solution (Wako, Tokyo, Japan).

2.8. Cross-sectional myofiber measurements

The left soleus, plantaris, gastrocnemius, and quadriceps muscles were removed, cleansed of extraneous tissue, and weighed. They were then placed in 4% PFA for 24 h and transferred to 70% ethanol until use in hematoxylin and eosin staining for morphological evaluation. Left-sided gastrocnemius and soleus muscles were transversely sectioned at the middle of the muscle belly at 5-μm thickness and stained with hematoxylin and eosin. An average of 300 myofibers was evaluated for morphological evaluation, and the myofiber cross-sectional area (CSA) was determined using ImageJ software (NIH) [24].

2.9. Microarray studies and data analyses

DNA microarray analyses were performed using a 3D-Gene system (Toray Industries, Kamakura, Kanagawa, Japan) as previously described [4,5,25]. Three mouse samples were used for each experiment. Genes were considered significant based on the criterion of > 2-fold (up- or downregulated) change.

2.10. Western blot analyses

Proteins (30 μg) isolated from adipose and muscular tissues of WT and KO mice were separated by sodium dodecyl sulfate-polyacrylamide gel electrophoresis (SDS-PAGE) and transferred to Immun-Blot polyvinylidene difluoride (PVDF) membranes (Bio-Rad Laboratories, K.K., Tokyo, Japan) using a semidry blotter. The blotted membranes were treated with 5% (*w/v*) skim milk in 10 mM Tris, 150 mM NaCl and 0.2% (*v/v*) Tween-20 and incubated overnight at 4 °C with the primary antibody. The following antibodies and dilutions were used: rabbit polyclonal antibodies to Gdf8 (dilution 1:1000; Abcam, Tokyo, Japan) and anti-GAPDH antibody (dilution 1:1000; Cell Signaling Technology, Tokyo, Japan). The membranes were then incubated for 45 min at room temperature with a peroxidase-conjugated secondary antibody and visualized using an ECL kit (GE Healthcare Bio-Science, Buckinghamshire, UK). Bands on Western blots were analyzed densitometrically using the Scion Image software program (version 4.0.2; Scion Corp., Frederick, MD, USA).

2.11. Immunofluorescence staining of muscular tissue

Gastrocnemius muscle sections were deparaffinized in xylene and ethanol. For the permeabilization step, we covered the tissue sections with ice-cold 100% methanol for 10 min at −20 °C. A blocking step was performed to reduce nonspecific staining by immersing the slides in 1% BSA/5% normal goat serum for 60 min. Immunofluorescence staining of Gdf8 was then carried out. For immunofluorescence staining, the sections were labeled with rabbit polyclonal antibodies to Gdf8 (Abcam, dilution 1:200), and then visualized with goat antirabbit IgG antibodies conjugated with Alexa Fluor dyes (green-stained) (Thermo Fisher, Tokyo, Japan, dilution 1:200).

2.12. Statistical analysis

All results are expressed as the mean ± SEM. An unpaired *t*-test was used to detect differences between the WT and KO mice. Differences were considered statistically significant at $p < 0.05$. All statistical analyses were performed with STATA/IC 14 (StataCorp, College Station, TX, USA) on a Macintosh computer.

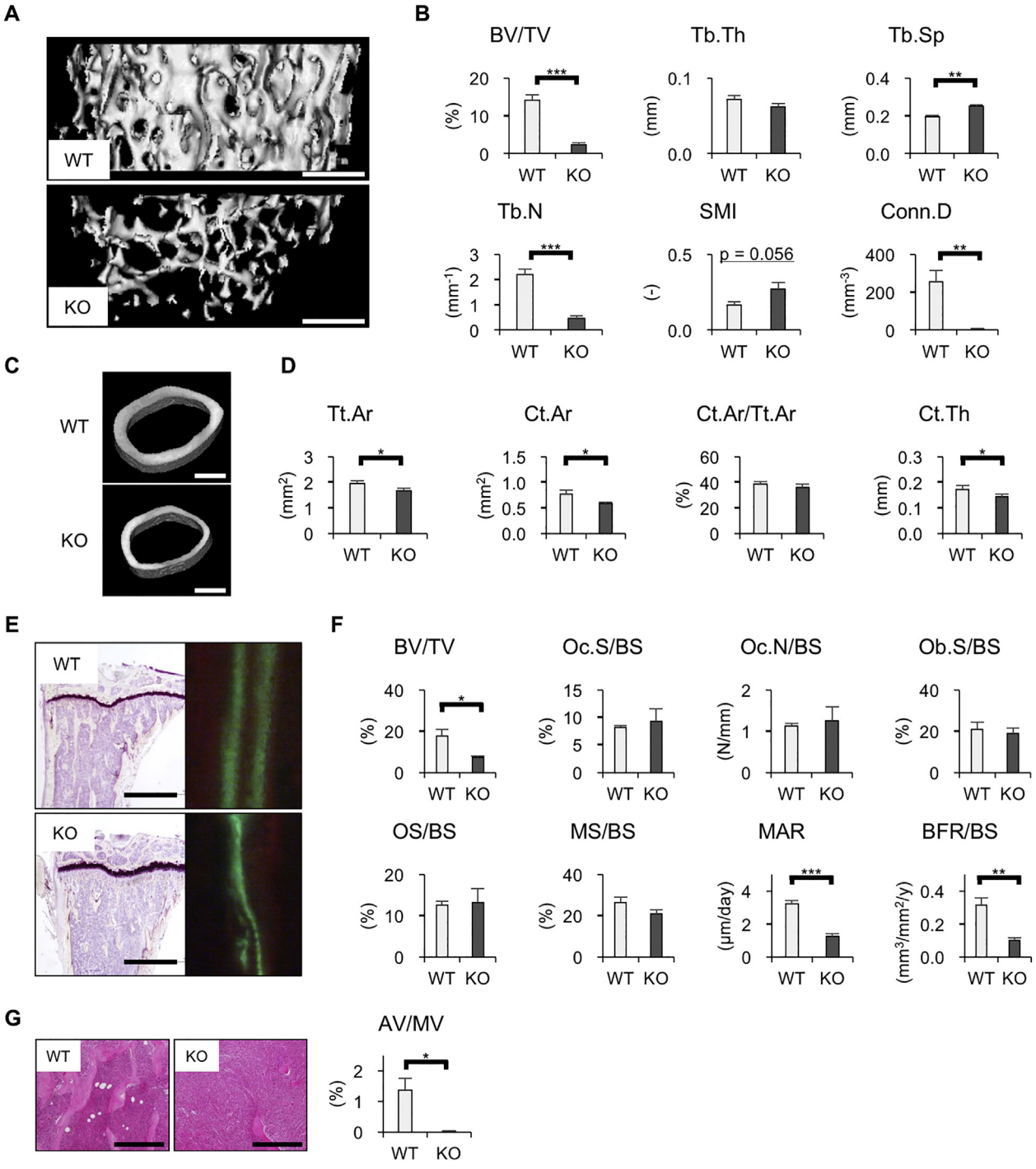

Fig. 1. Analyses of static and dynamic bone histomorphometry.
(A) Three-dimensional imaging and (B) microstructure parameters of the trabecular bone as measured by micro-CT: bone volume, BV/TV; trabecular thickness, Tb.Th; trabecular separation, Tb.Sp; trabecular number, Tb.N; structure model index, SMI; and connectivity density, Conn.D. Scale bar = 500 μm. (C) Three-dimensional imaging and (D) parameters of the cortical bone as measured by micro-CT: total cross-sectional area inside the periosteal envelope; Tt.Ar; cortical bone area; Ct.Ar; cortical area fraction; and Ct.Ar/Tt.Ar; average cortical thickness, Ct.Th. Scale bar = 500 μm. (E) Light and fluorescence microscopic imaging of the nondecalcified specimens. Scale bar = 1 mm. (F) The histomorphometric parameters were as follows: bone volume, BV/TV; osteoclast surface, Oc.S/BS; osteoclast number, Oc.N/BS; osteoblast surface, Ob.S/BS; osteoid surface, OS/BS; mineralizing surface, MS/BS; mineral apposition rate, MAR; and bone formation rate, BFR/BS. (G) H&*E*-stained images and parameters of adipose tissue volume in bone marrow: adipose tissue volume per total marrow volume, AV/MV. Scale bar = 250 μm. (n = 5 in each group). Data are shown as the mean ± SEM. *p < 0.05, **p < 0.01, and ***p < 0.001.

3. Results

3.1. Deletion of Wnt10a decreases osteogenic activity and adipogenesis in bone marrow

Micro-CT imaging showed significant differences in the trabecular bone of the distal femur (Fig. 1A). Regarding the microstructural parameters of the trabecular bone at the distal femur, the trabecular BV/TV, Tb.N and Conn.D in the KO group were significantly lower than those in the WT group, and the Tb.Sp in the KO group was significantly higher than that in the WT group (Fig. 1B). Regarding the parameters of the cortical bone at the femur midshaft, the Tt.Ar, Ct.Ar and Ct.Th in the KO group were significantly lower than those in the WT group, and there was no significant difference in the Ct.Ar/Tt.Ar between the KO and WT groups (Fig. 1C and D).

Regarding the static and dynamic bone histomorphometry of the trabecular bone at the proximal tibiae, the BV/TV, MAR and BFR/BS in the KO group were significantly lower than those in the WT group (Figs. 1E and F), and there were no significant differences in the Oc.S/BS, Oc.N/BS, Ob.S/BS, OS/BS and MS/BS between the WT and KO groups (Fig. 1F). The value of AV/MV in the KO group was significantly lower than that in the WT group (Fig. 1G).

For the cell culture, the area stained by Alizarin Red was significantly smaller and the number of Oil Red O-positive colonies per well was significantly lower in the KO group than in the WT group, although there was no significant difference in the number of total or ALP-positive CFU-f between the WT and KO groups (Figures 2Aand 2B). Regarding mRNA expression in the bone marrow cells obtained from the femur, the levels of β-catenin, RUNX2, Col1a1, osteocalcin, PPARγ and FABP4 in the KO group were significantly lower than those in the WT group (Fig. 2C).

3.2. Deletion of Wnt10a decreases the white/brown adipose tissue weight and promotes beige adipogenesis in subcutaneous fat

Inguinal, gonadal and brown adipose tissue weights normalized by body weight in the KO group were significantly decreased compared with those in the WT group (Fig. 3A). The proportions of visceral and subcutaneous fat in the KO group were significantly lower than those in the WT group (Fig. 3B and C). Samples of inguinal adipose tissue from the KO group showed beige adipogenesis (Fig. 3D). The gene expression levels of beige adipogenesis markers, such as Cidea, Cox5b, Dio2, Elovl3 and UCP1, in the inguinal adipose tissue of the KO group were significantly higher than those of the WT group, except PRDM16 (Fig. 3E).

3.3. Muscle weight is not decreased in Wnt10a KO mice

No significant differences were observed in the quadriceps, gastrocnemius, plantaris and soleus muscle weights normalized by body weight in both groups (Fig. 4A). The CSA of 300 muscle fibers in the gastrocnemius muscles of the KO group tended to be larger than that of the WT group ($p = 0.086$, Figs. 4B), while the 300-fiber CSA in the soleus of the KO group was significantly larger than that of the WT group. The protein expression of β-catenin appeared to be low in the KO group (Fig. 4C). The mRNA expression level of MyHC in the gastrocnemius and soleus muscles of the KO group was significantly higher than that of the WT group. Regarding the gastrocnemius, there were no significant differences in muscle atrophic markers (atrogin-1, MuRF1) and muscle differentiation markers (Myf5, MyoD, myogenin) between the two groups. On the other hand, the mRNA expression levels of MyoD and myogenin in the soleus of the KO group were significantly higher than those of the WT group (Fig. 4D).

3.4. Gdf8/myostatin expression is decreased in adipose and muscle tissues of Wnt10a KO mice

cDNA expression array analyses were performed to compare skin tissue samples obtained from WT and KO mice. The Wnt10a and Gdf8 genes showed significant downregulation in the KO group (Fig. 5A). The Gdf8 levels in inguinal adipose tissue (Fig. 5B-D) and gastrocnemius muscle tissue (Fig. 5E-G) in the KO group were significantly lower than those in the WT group.

4. Discussion

The results of this study are summarized in Fig. 6, and the new findings are as follows: 1) This study was the first to histologically investigate the bone, fat and muscle phenotypes in Wnt10a KO mice. Dynamic bone histomorphometry was also performed on trabecular bone using fluorescent labels. 2) A decrease in trabecular bone mass with impaired bone formation was observed. In particular, the decrease in mineralized activity was remarkable. 3) The amount of fat marrow was decreased, suggesting a decline in adipocyte differentiation in bone marrow cells. 4) The number of white adipocytes in subcutaneous fat mass was decreased, while that of beige adipocytes in subcutaneous fat was increased. 5) The expression of GDF8/myostatin was decreased in adipose tissue and muscle tissue.

Static and dynamic histomorphometry analysis of the cancellous bone from the lower limbs of the KO mice showed degradation of the bone microstructure (BV/TV, Tb.N, Tb.Sp, Conn.D) and a decrease in the MAR and BFR/BS. The amount of adipose tissue in the bone marrow was also decreased. In the primary cultures of bone marrow cells, the Alizarin Red-stained area and the Oil Red O-positive colony count were decreased, indicating a decline in mineralization and adipocyte differentiation. Fat mass, including both subcutaneous and visceral fat, in KO mice decreased, and brown fat in the scapular region was also reduced. White adipocytes in the subcutaneous fat were converted to beige adipocytes, and the expression of beige adipogenesis markers (Cidea, Cox5b, Dio2, Elovl3, UCP1) also increased. However, the muscle weight of the lower limbs was not decreased in the KO group, and the 300-fiber CSA of soleus muscle was larger than that in the control group. There were no changes in Myf 5 expression, and the expression of muscle differentiation markers (MyoD, myogenin) and MyHC in soleus muscle was elevated in the KO group. Furthermore, the expression levels of Gdf8/myostatin, which is an important factor for the adjustment of muscle and fat mass, in the subcutaneous fat and gastrocnemius muscles of the KO mice were significantly lower than those of the control mice. The above points will be discussed below.

Wnt10a KO mice showed a marked reduction in the bone and fat mass of bone marrow tissue due to a decline in osteogenic potential and adipose differentiation. In primary cultures of bone marrow cells, mineralization decreased without a decline in osteoblastogenesis, while adipogenic differentiation significantly decreased. Cawthorn et al. [6] reported that Wnt6, Wnt10a and Wnt10b inhibit adipogenesis and stimulate osteoblastogenesis through a β-catenin-dependent mechanism. In addition, Chen et al. [7] reported that inhibiting DNA methylation switches adipogenesis to osteoblastogenesis by activating Wnt10a. In the above studies, the effect of Wnt10a on osteoblastogenesis and adipogenesis had opposite results, and the findings of this study, which showed the decline of osteogenic activity and adipogenesis, are not consistent with the results of previous in vitro studies. These findings suggest that Wnt10a may have indirect effects, in addition to direct effects, on bone and fat in vivo.

Adipogenesis in the bone marrow tissue of Wnt10a KO mice was decreased, whereas beige adipogenesis in the subcutaneous adipose tissue was strongly promoted. The adipose tissue in the groin that should be composed of white adipocytes showed UCP1 positivity, an indicator of beige adipocytes, in the immunohistochemically stained specimens, and the expression of beige adipogenesis markers, except for

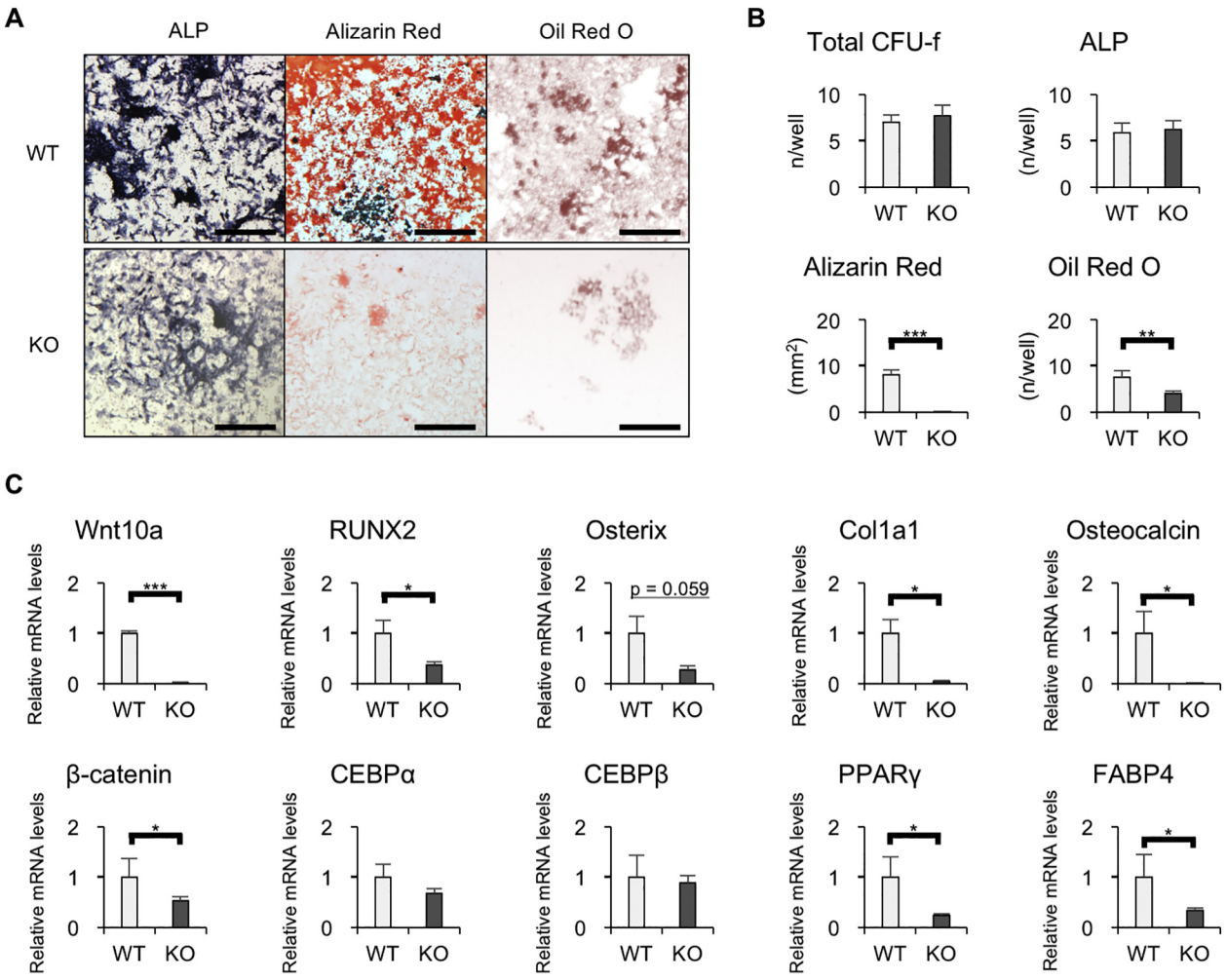

Fig. 2. Assays using bone marrow cells.

Osteogenic and adipogenic potentials are evaluated in primary cultures of bone marrow cells. (A) Photographs of alkaline phosphatase (ALP)-, Alizarin Red- and Oil Red O-stained colonies. Scale bar = 500 μm. (B) Number of total, ALP-positive CFU-f, and Oil Red O-positive colonies as well as the Alizarin Red-stained area per well. (C) mRNA expression levels of Wnt10a, β-catenin, and osteoblastogenesis-, osteogenesis- and adipogenesis-related markers in bone marrow cells obtained from the femur ($n = 5$ in each group). Data are shown as the mean ± SEM. $^{*}p < 0.05$, $^{**}p < 0.01$, and $^{***}p < 0.001$. (For interpretation of the references to color in this figure legend, the reader is referred to the web version of this article.)

PRDM16, was also increased. Why the expression of PRDM16, a beige adipogenesis marker, was decreased is unknown, but PRDM16 is an important molecule that switches cell fate between muscle and brown adipose tissue [26]. Since the amount of brown adipose tissue in Wnt10a KO mice was also significantly decreased compared to that in WT mice, regulation of PRDM16 expression through Wnt10a or modulation of muscle/brown adipose tissue differentiation mechanisms may have occurred in those mice. There is no evidence of a relationship between beige adipogenesis and the Wnt10a gene, but sclerostin, which suppresses WNT signals, was reported to contribute to beige adipogenesis of white adipocytes [8], and this finding did not contradict the results of our study.

In general, since bone and muscle are strongly related [9,27,28], muscle mass is expected to decrease with bone loss. However, the weight of the lower limb muscles of Wnt10a KO mice was not decreased compared with that of WT mice. There was also no muscle fiber atrophy on H&E-stained sections of the gastrocnemius muscle and no elevation of muscle atrophy markers (atrogin-1, MuRF1) in those tissues. The 300-fiber CSA of the KO group was larger than that of the WT group, and increased expression of myosin heavy chain was observed in the gastrocnemius and soleus muscles. The effects of Wnt10a deficiency on some muscle phenotypes were soleus muscle dominant. The soleus muscle is a muscle rich in type I muscle fiber (slow twitch) and contains many mitochondria in the muscle fibers. There is a close relationship between Wnt10a and mitochondrial function [29], and plasma 8-OHdG produced mainly in mitochondria is positively correlated with plasma myostatin in rat [30]. Thus, the phenotype of the soleus muscle caused by deficiency of Wnt10a may be related to the mitochondrial dysfunction.

In addition, the expression of Gdf8/myostatin in the subcutaneous fat and gastrocnemius muscle of Wnt10a KO mice was significantly decreased. Based on the above results, we speculated that the regulation of Gdf8 expression by the Wnt10a gene may be involved in maintaining muscle mass in Wnt10a KO mice (Fig. 6). The relationships between myostatin expression and the in vivo phenotype were not examined in this study, as those relationships have already been reported in studies of the adipose tissue and skeletal muscle of myostatin KO mice [31–33]. Gdf8/myostatin KO mice exhibited a marked increase in muscle mass and a decrease in fat mass [34], which may promote beige adipogenesis in white adipocytes [35]. We found no conflicting results in the data from this study; however, there was no evidence of a relationship between Gdf8/myostatin and the Wnt10a gene. Thus, it is necessary to discuss the mechanism by which Wnt10a regulates GDf8. Several reports have noted an association between Gdf8/myostatin and

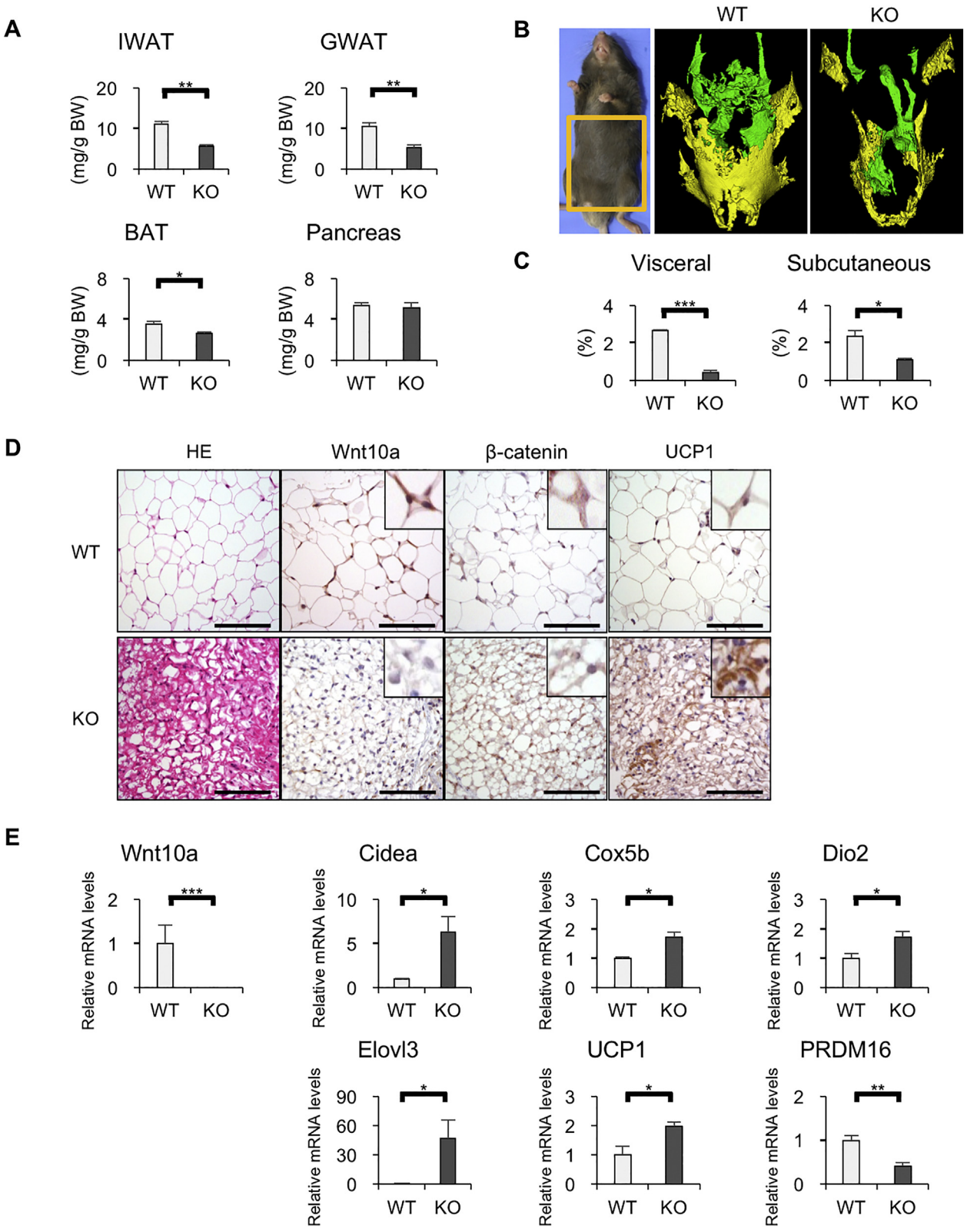

Fig. 3. Analysis of adipose tissue.
(A) Weights of inguinal white adipose tissue (IWAT), gonadal white adipose tissue, brown adipose tissue at the scapular region (BAT) and pancreas. (n = 6 in each group) (B) Representative 3D images of abdominal and pelvic micro-CT show the visceral (*green* in color) and subcutaneous fat (*yellow* in color). The fat volume in mice was measured from the base of the ensiform cartilage to the pelvic floor (areas surrounded by *orange* lines). (C) Visceral and subcutaneous fat percentage per total volume from the base of the ensiform cartilage to the pelvic floor. (n = 5 in each group) (D) Representative H&E-stained and Wnt10a-, β-catenin- and UCP1-IHC-stained sections in IWAT. Scale bar = 100 μm. (E) The gene expression of Wnt10a and beige adipogenesis markers in IWAT. (n = 5 in each group). Data are shown as the mean ± SEM. *p < 0.05, **p < 0.01, and ***p < 0.001. (For interpretation of the references to color in this figure legend, the reader is referred to the web version of this article.)

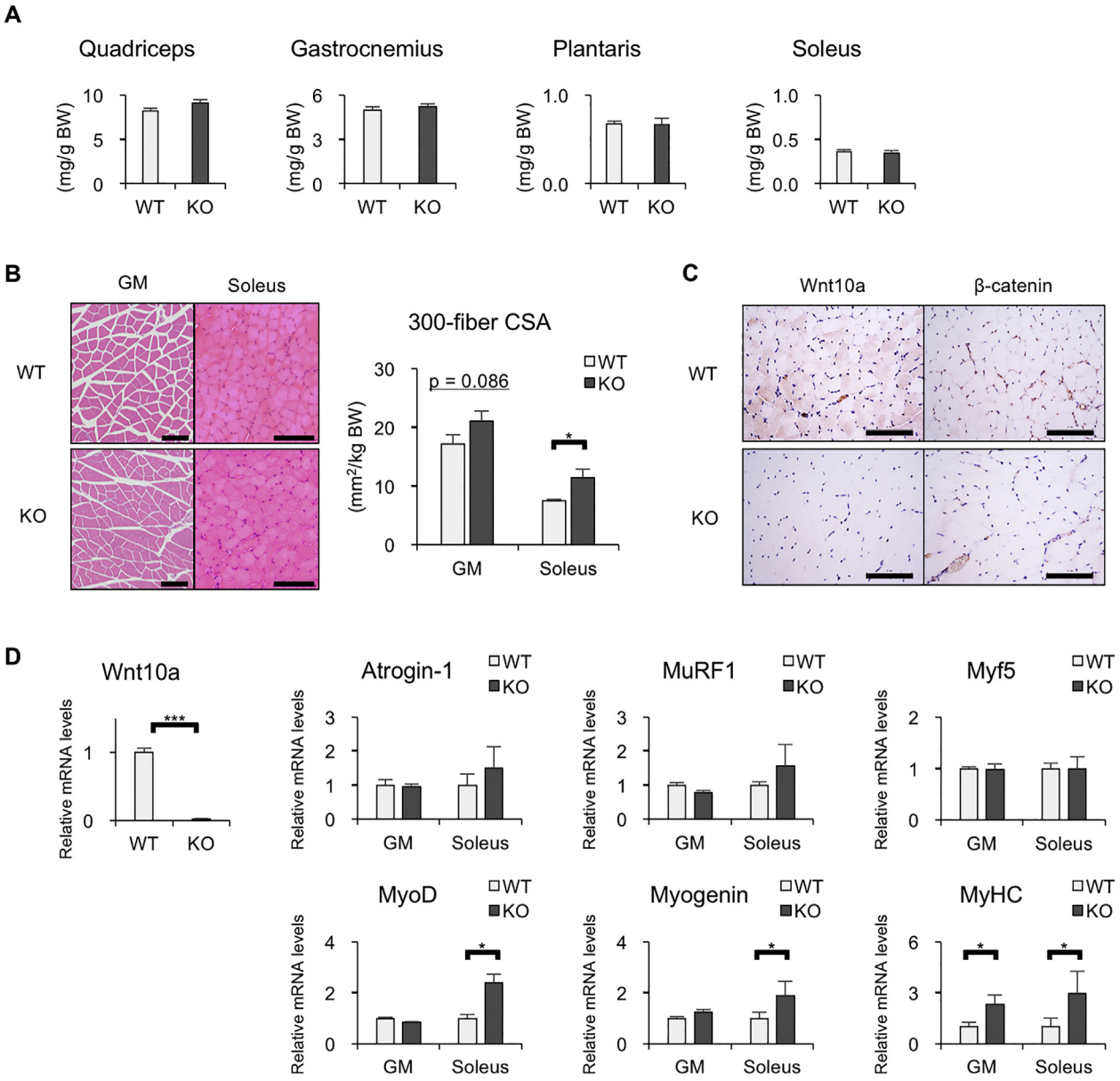

Fig. 4. Analysis of muscular tissue.
(A) Weight of the quadriceps, gastrocnemius, plantaris and soleus muscles. (B) Light microscope images of H&E-stained sections of the gastrocnemius muscle. Scale bar = 100 μm. The 300-muscle fiber cross-sectional areas (CSAs) of the gastrocnemius and soleus muscles normalized by body weight (n = 5 in each group). (C) Representative Wnt10a and β-catenin IHC-stained sections of the gastrocnemius and soleus muscles. Scale bar = 100 μm. (D) Gene expression levels of Wnt10a in the gastrocnemius muscle and the following muscle-related markers in the gastrocnemius and soleus muscles; atrogin-1, MuRF1, Myf5, MyoD, myogenin and MyHC. Data are shown as the mean ± SEM (n = 5 in each group); $^{*}p < 0.05$.

Wnt signaling [36,37]. Reports by Takata et al. suggested that Wnt4 antagonizes myostatin [38]. By using a CAGA reporter assay, Bernardi et al. confirmed the inhibition of the myostatin-activated Smad signaling pathway by Wnt4 [39]. In addition, a study of lithium chloride (activation of Wnt/β-catenin signaling) strongly suggested that Wnt4 negatively regulates myostatin expression through activation of the canonical β-catenin pathway. It is possible that Wnt10a also regulates myostatin expression/signaling through activation of the canonical β-catenin pathway or noncanonical pathway. Further research is needed to determine the mechanism by which Wnt10a regulates GDF8/myostatin and to determine the in vivo effect of the Wnt10a gene on bone, fat and muscle.

This study has some limitations. We did not consider the influence of Wnt10a gene deficiency at the time of embryogenesis and growth. Wnt10a mice have a low fertility rate and are difficult to study. Moreover, since the Wnt10a KO mice used in this study were not conditional knockout mice, the influence of Wnt10a gene deficiency in the embryonic and growth phases of bone, fat and muscle cannot be completely eliminated. In the future, analysis using conditional knockout mice may be necessary.

5. Conclusions

In conclusion, trabecular bone loss in the lower limbs of Wnt10a mice occur with a decrease in bone mineralization ability. The amount of adipose tissue in the bone marrow was also decreased, and the adipocyte differentiation ability was reduced. The inguinal, gonadal, and scapular fat mass in the Wnt10a KO mice was decreased, and white adipocytes in the subcutaneous fat were converted to beige adipocytes. The muscle weight of the lower limbs was not decreased, and no muscle

A

Gene Symbol	Accession number	KO/WT	Gene description
Wnt10a	NM_009518	0.06	wingless related MMTV integration site 10a
Gdf8/myostatin	NM_010834	0.16	growth differentiation factor 8

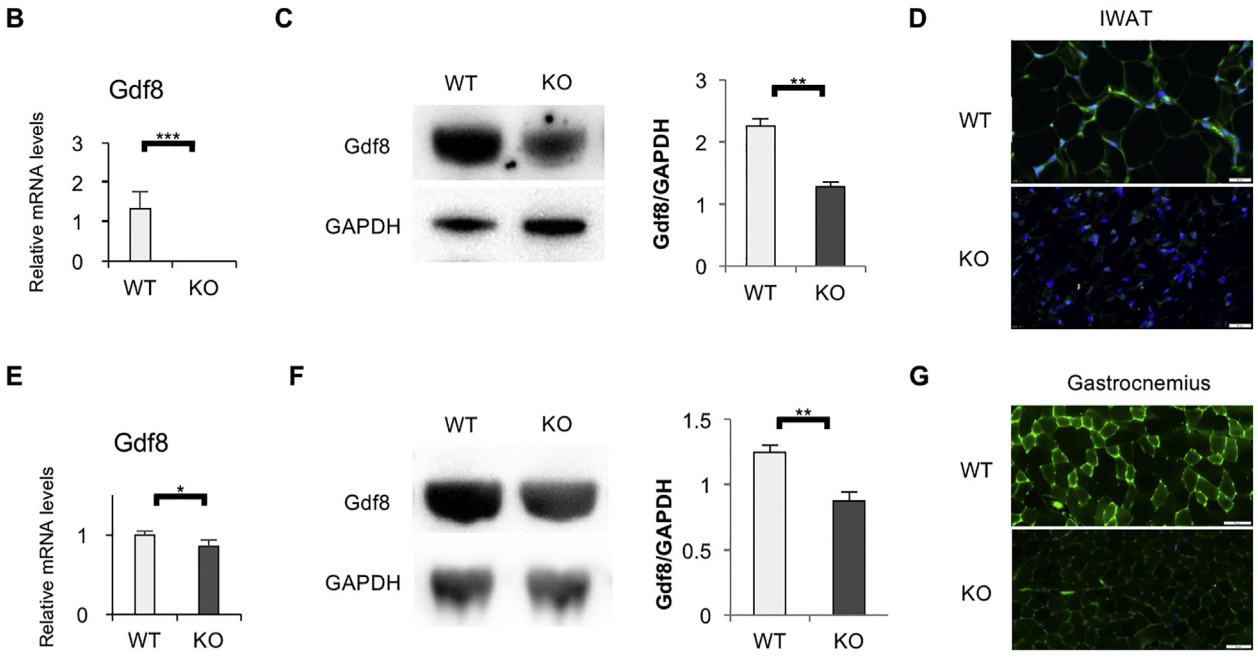

Fig. 5. Analysis of Gdf8/myostatin expression.
(A) DNA microarray analyses of the skin. (B) mRNA expression analysis (n = 5 in each group), (C) Western blotting analysis (n = 5 in each group) and (D) fluorescence-stained imaging of inguinal white adipose tissue. Scale bar = 20 μm. (E) mRNA expression (*n* = 7 in each group), (F) Western blotting analysis (n = 5 in each group) and (G) images of fluorescence-stained gastrocnemius muscle. Scale bar = 50 μm. Data are shown as the mean ± SEM. *p < 0.05, **p < 0.01, and ***p < 0.001.

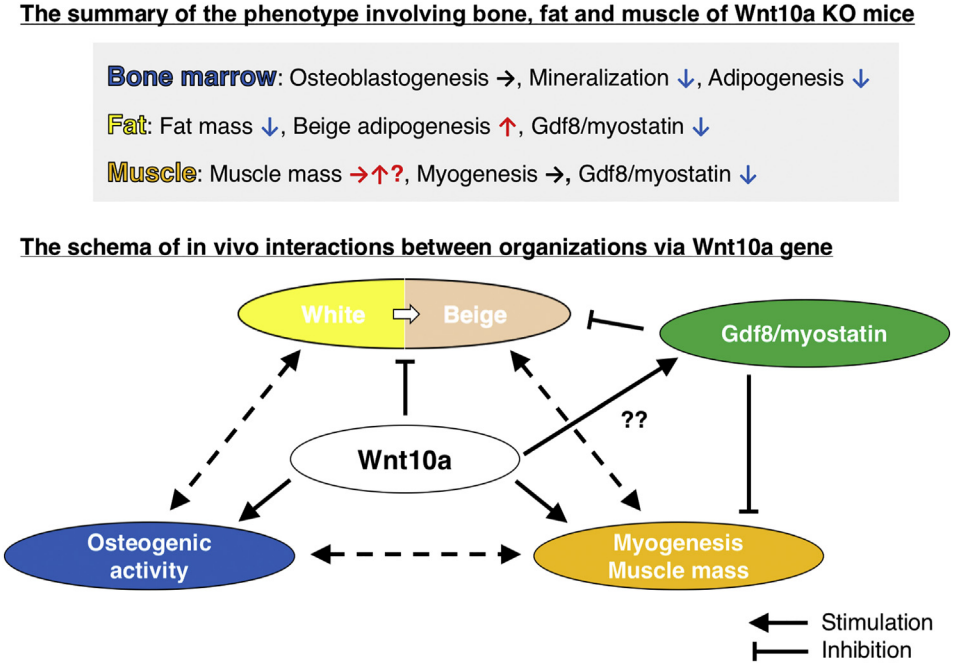

Fig. 6. Summary of Wnt10a KO mice and the schema of in vivo interactions among bone, fat and muscle via Wnt10a.

fiber atrophy was observed in the tissue sections. In the subcutaneous fat and gastrocnemius muscle, the expression of Gdf8/myostatin, an important factor related to the regulation of fat/muscle mass, was decreased, suggesting that Wnt10a may mediate the regulation of Gdf8/myostatin expression. This study was the first to histologically evaluate the bone, fat and muscle phenotypes of Wnt10a KO mice. The results obtained by investigating the three tissues together could help to elucidate the in vivo interactions of the Wnt10a gene in the future.

Disclosures

The authors report that there are no conflicts of interest.

Acknowledgments

We would like to thank Ryoko Maekado (Shared-Use Research Center, School of Medicine, University of Occupational and Environmental Health) for her expert technical assistance.

References

[1] L. Adaimy, E. Chouery, H. Megarbane, S. Mroueh, V. Delague, E. Nicolas, et al., Mutation in WNT10A is associated with an autosomal recessive ectodermal dysplasia: the odonto-onycho-dermal dysplasia, Am. J. Hum. Genet. 81 (4) (Oct 2007) 821–828 (Epub 2007/09/12).
[2] M. Xu, J. Horrell, M. Snitow, J. Cui, H. Gochnauer, C.M. Syrett, et al., WNT10A mutation causes ectodermal dysplasia by impairing progenitor cell proliferation and KLF4-mediated differentiation, Nat. Commun. 8 (Jun 7 2017) 15397 (Epub 2017/06/08).
[3] J. Yang, S.K. Wang, M. Choi, B.M. Reid, Y. Hu, Y.L. Lee, et al., Taurodontism, variations in tooth number, and misshapened crowns in Wnt10a null mice and human kindreds, Mol. Genet. Genomic Med. 3 (1) (Jan 2015) 40–58 (Epub 2015/01/30).
[4] K.Y. Wang, S. Yamada, H. Izumi, M. Tsukamoto, T. Nakashima, T. Tasaki, et al., Critical in vivo roles of WNT10A in wound healing by regulating collagen expression/synthesis in WNT10A-deficient mice, PLoS One 13 (3) (2018) e0195156(Epub 2018/03/30).
[5] Y. Yasuniwa, H. Izumi, K.Y. Wang, S. Shimajiri, Y. Sasaguri, K. Kawai, et al., Circadian disruption accelerates tumor growth and angio/stromagenesis through a Wnt signaling pathway, PLoS One 5 (12) (Dec 23 2010) e15330(Epub 2011/01/05).
[6] W.P. Cawthorn, A.J. Bree, Y. Yao, B. Du, N. Hemati, G. Martinez-Santibanez, et al., Wnt6, Wnt10a and Wnt10b inhibit adipogenesis and stimulate osteoblastogenesis through a beta-catenin-dependent mechanism, Bone 50 (2) (Feb 2012) 477–489 (Epub 2011/08/30).
[7] Y.S. Chen, R. Wu, X. Yang, S. Kou, O.A. MacDougald, L. Yu, et al., Inhibiting DNA methylation switches adipogenesis to osteoblastogenesis by activating Wnt10a, Sci. Rep. 6 (May 3 2016) 25283 (Epub 2016/05/04).
[8] K. Fulzele, F. Lai, C. Dedic, V. Saini, Y. Uda, C. Shi, et al., Osteocyte-secreted Wnt signaling inhibitor Sclerostin contributes to Beige Adipogenesis in peripheral fat depots, J. Bone Miner. Res. 32 (2) (Feb 2017) 373–384 (Epub 2016/09/23).
[9] M.A. Rudnicki, B.O. Williams, Wnt signaling in bone and muscle, Bone 80 (Nov 2015) 60–66 (Epub 2015/10/11).
[10] M.L. Bouxsein, S.K. Boyd, B.A. Christiansen, R.E. Guldberg, K.J. Jepsen, R. Muller, Guidelines for assessment of bone microstructure in rodents using micro-computed tomography, J. Bone Miner. Res. 25 (7) (Jul 2010) 1468–1486 (Epub 2010/06/10).
[11] M. Kina-Tanada, M. Sakanashi, A. Tanimoto, T. Kaname, T. Matsuzaki, K. Noguchi, et al., Long-term dietary nitrite and nitrate deficiency causes the metabolic syndrome, endothelial dysfunction and cardiovascular death in mice, Diabetologia 60 (6) (Jun 2017) 1138–1151 (Epub 2017/03/30).
[12] M. Tsukamoto, K. Menuki, T. Murai, A. Hatakeyama, S. Takada, K. Furukawa, et al., Elcatonin prevents bone loss caused by skeletal unloading by inhibiting preosteoclast fusion through the unloading-induced high expression of calcitonin receptors in bone marrow cells, Bone 85 (Apr 2016) 70–80 (Epub 2016/02/07).
[13] A.M. Parfitt, M.K. Drezner, F.H. Glorieux, J.A. Kanis, H. Malluche, P.J. Meunier, et al., Bone histomorphometry: standardization of nomenclature, symbols, and units. Report of the ASBMR Histomorphometry nomenclature committee, J. Bone Miner. Res. Off. J. Am. Soc. Bone Miner. Res. 2 (6) (Dec 1987) 595–610 (Epub 1987/12/01).
[14] D.W. Dempster, J.E. Compston, M.K. Drezner, F.H. Glorieux, J.A. Kanis, H. Malluche, et al., Standardized nomenclature, symbols, and units for bone histomorphometry: a 2012 update of the report of the ASBMR Histomorphometry nomenclature committee, J. Bone Miner. Res. 28 (1) (Jan 2013) 2–17 (Epub 2012/12/01).
[15] T. Sakata, A. Sakai, H. Tsurukami, N. Okimoto, Y. Okazaki, S. Ikeda, et al., Trabecular bone turnover and bone marrow cell development in tail-suspended mice, J. Bone Miner. Res. 14 (9) (Sep 1999) 1596–1604 (Epub 1999/09/01).
[16] A. Sakai, T. Sakata, S. Tanaka, R. Okazaki, N. Kunugita, T. Norimura, et al., Disruption of the p53 gene results in preserved trabecular bone mass and bone formation after mechanical unloading, J. Bone Miner. Res. 17 (1) (Jan 2002) 119–127 (Epub 2002/01/05).
[17] M. Watanuki, A. Sakai, T. Sakata, H. Tsurukami, M. Miwa, Y. Uchida, et al., Role of inducible nitric oxide synthase in skeletal adaptation to acute increases in mechanical loading, J. Bone Miner. Res. 17 (6) (Jun 2002) 1015–1025 (Epub 2002/06/11).
[18] K.F. Okuma, K. Menuki, M. Tsukamoto, T. Tajima, H. Fukuda, Y. Okada, et al., Disruption of the aldehyde dehydrogenase 2 gene results in no increase in trabecular bone mass due to skeletal loading in association with impaired cell cycle regulation through p21 expression in the bone marrow cells of mice, Calcif. Tissue Int. 101 (3) (Sep 2017) 328–340 (Epub 2017/05/06).
[19] T. Mori, N. Okimoto, A. Sakai, Y. Okazaki, N. Nakura, T. Notomi, et al., Climbing exercise increases bone mass and trabecular bone turnover through transient regulation of marrow osteogenic and osteoclastogenic potentials in mice, J. Bone Miner. Res. 18 (11) (Nov 2003) 2002–2009 (Epub 2003/11/11).
[20] T. Tsuchiya, A. Sakai, K. Menuki, T. Mori, Y. Takeuchi, S. Kanoh, et al., Disruption of aldehyde dehydrogenase 2 gene results in altered cortical bone structure and increased cortical bone mineral density in the femoral diaphysis of mice, Bone 53 (2) (Apr 2013) 358–368 (Epub 2013/01/15).
[21] K. Menuki, T. Mori, A. Sakai, M. Sakuma, N. Okimoto, Y. Shimizu, et al., Climbing exercise enhances osteoblast differentiation and inhibits adipogenic differentiation with high expression of PTH/PTHrP receptor in bone marrow cells, Bone 43 (3) (Sep 2008) 613–620 (Epub 2008/06/24).
[22] A. Hatakeyama, S. Uchida, H. Utsunomiya, M. Tsukamoto, H. Nakashima, E. Nakamura, et al., Isolation and characterization of synovial mesenchymal stem cell derived from hip joints: a comparative analysis with a matched control knee group, Stem Cells Int. 2017 (2017) 9312329 (Epub 2017/01/25).
[23] T. Tajima, K. Menuki, K.F. Okuma, M. Tsukamoto, H. Fukuda, Y. Okada, et al., Cortical bone loss due to skeletal unloading in aldehyde dehydrogenase 2 gene knockout mice is associated with decreased PTH receptor expression in osteocytes, Bone 110 (May 2018) 254–266 (Epub 2018/02/27).
[24] Y. Jeong, S.M. Carleton, B.A. Gentry, X. Yao, J.A. Ferreira, D.J. Salamango, et al., Hindlimb skeletal muscle function and skeletal quality and strength in +/G610C mice with and without weight-bearing exercise, J. Bone Miner. Res. 30 (10) (Oct 2015) 1874–1886 (Epub 2015/04/02).
[25] H. Noguchi, S. Yamada, A. Nabeshima, X. Guo, A. Tanimoto, K.Y. Wang, et al., Depletion of apoptosis signal-regulating kinase 1 prevents bile duct ligation-induced necroinflammation and subsequent peribiliary fibrosis, Am. J. Pathol. 184 (3) (Mar 2014) 644–661 (Epub 2014/01/15).
[26] P. Seale, B. Bjork, W. Yang, S. Kajimura, S. Chin, S. Kuang, et al., PRDM16 controls a brown fat/skeletal muscle switch, Nature 454 (7207) (Aug 21 2008) 961–967 (Epub 2008/08/23).
[27] D.D. Bikle, C. Tahimic, W. Chang, Y. Wang, A. Philippou, E.R. Barton, Role of IGF-I signaling in muscle bone interactions, Bone 80 (Nov 2015) 79–88 (Epub 2015/10/11).
[28] C.A. Goodman, T.A. Hornberger, A.G. Robling, Bone and skeletal muscle: key players in mechanotransduction and potential overlapping mechanisms, Bone 80 (Nov 2015) 24–36 (Epub 2015/10/11).
[29] E. Berger, E. Rath, D. Yuan, N. Waldschmitt, S. Khaloian, M. Allgauer, et al., Mitochondrial function controls intestinal epithelial stemness and proliferation, Nat. Commun. 7 (Oct. 2016) 13171.
[30] K.G. Avin, N.X. Chen, J.M. Organ, C. Zarse, K. O'Neill, R.G. Conway, R.J. Konrad, R.L. Bacallao, M.R. Allen, S.M. Moe, Skeletal muscle regeneration and oxidative stress are altered in chronic kidney disease, PLoS One 11 (8) (Aug 2016) e0159411.
[31] A.C. McPherron, A.M. Lawler, S.J. Lee, Regulation of skeletal muscle mass in mice by a new TGF-beta superfamily member, Nature 387 (6628) (May 1997) 83–90.
[32] J. Lin, H.B. Arnold, M.A. Della-Fera, M.J. Azain, D.L. Hartzell, C.A. Baile, Myostatin knockout in mice increases myogenesis and decreases adipogenesis, Biochem. Biophys. Res. Commun. 291 (3) (Mar 2002) 701–706.
[33] A.C. McPherron, S.J. Lee, Suppression of body fat accumulation in myostatin-deficient mice, J. Clin. Invest. 109 (5) (Mar 2002) 595–601.
[34] M.N. Elkasrawy, M.W. Hamrick, Myostatin (GDF-8) as a key factor linking muscle mass and bone structure, J. Musculoskelet. Neuronal Interact. 10 (1) (Mar 2010) 56–63 (Epub 2010/03/02).
[35] T. Shan, X. Liang, P. Bi, S. Kuang, Myostatin knockout drives browning of white adipose tissue through activating the AMPK-PGC1alpha-Fndc5 pathway in muscle, FASEB J. 27 (5) (May 2013) 1981–1989 (Epub 2013/01/31).
[36] W. Guo, J. Flanagan, R. Jasuja, J. Kirkland, L. Jiang, S. Bhasin, The effects of myostatin on adipogenic differentiation of human bone marrow-derived mesenchymal stem cells are mediated through cross-communication between Smad3 and Wnt/beta-catenin signaling pathways, J. Biol. Chem. 283 (14) (Apr 2008) 9136–9145.
[37] J.M. Tee, C. van Rooijen, R. Boonen, D. Zivkovic, Regulation of slow and fast muscle myofibrillogenesis by Wnt/beta-catenin and myostatin signaling, PLoS One 4 (6) (Jun 2009) e5880.
[38] H. Takata, K. Terada, H. Oka, Y. Sunada, T. Moriguchi, T. Nohno, Involvement of Wnt4 signaling during myogenic proliferation and differentiation of skeletal muscle, Dev. Dyn. 236 (10) (Oct 2007) 2800–2807.
[39] H. Bernardi, S. Gay, Y. Fedon, B. Vernus, A. Bonnieu, F. Bacou, Wnt4 activates the canonical beta-catenin pathway and regulates negatively myostatin: functional implication in myogenesis, Am. J. Phys. Cell Phys. 300 (5) (May 2011) C1122–C1138.